Monte Carlo Simulations of Disjoining-Pressure Isotherms for Lennard−Jones Surfactant-Stabilized Free Thin Films

Divesh Bhatt, John Newman, and C. J. Radke*

Department of Chemical Engineering, University of California, Berkeley, California 94720-1462

Received: March 31, 2004; In Final Form: June 11, 2004

We present Monte Carlo simulations of disjoining-pressure isotherms for soluble-surfactant-stabilized free thin films. To mimic actual experiments, we define a disjoining-pressure isotherm such that films of all thicknesses on that isotherm are in equilibrium with the same infinite reservoir of surfactant and solvent. This necessitates use of inert-gas molecules to vary the film thicknesses while still maintaining equilibrium with the reservoir. All types of molecules in the system (solvent, surfactant, and inert gas) are defined by using Lennard−Jones (LJ) based potentials. For thick films, the center of the film is sufficiently far away from the interface for the surfactant orientation to be random, whereas at the interface, the surfactant molecules are elongated and oriented roughly perpendicular to the interface. As the films are thinned, the disjoining pressure (Π) is positive and increases monotonically. Two bulk surfactant concentrations are considered that differ by a factor of about 2. For the isotherm with a higher surfactant concentration, the disjoining pressure is larger in magnitude due to higher surface coverage and concomitant stretching of the adsorbed surfactant, but the difference is not substantial within the accuracy of our simulations.

Introduction

A thin liquid film of a few tens of nanometers in thickness and bounded on both sides by gas or vapor (and hence, a free liquid thin film) is of importance in systems such as foams where typical aqueous surfactant- and/or polymer-stabilized films are surrounded by air. In thin liquid films, the normal component of pressure is constant across the interface, whereas the tangential component varies as a function of position perpendicular to the liquid/vapor interface.[1−3] However, the constant normal pressure in the film region is not the same as the isotropic pressure in the bulk liquid with which the film is in contact. The difference between these two pressures is the disjoining pressure, Π.[2,3] When reported as a function of film thickness, h, at constant temperature, $\Pi(h)$ is called the disjoining-pressure isotherm. Foam (and emulsion) stability is, in large measure, determined by the disjoining-pressure isotherm.[4,5]

Numerous experimental studies are available for the disjoining-pressure isotherms of aqueous thin films containing surfactants,[6−13] and a few for aqueous films stabilized with proteins[14,15] and polyelectrolytes.[16] Likewise, there are systematic molecular simulations available[17−25] of the forces in confined thin films (i.e., confined between solid walls). However, despite known differences in the types of film forces occurring in hard and soft films,[26] molecular simulations of the forces in free thin liquid films are almost nonexistent.[27,28] Long wavelength fluctuations (i.e., due to thermal capillary waves) in systems with free interfaces tend to destabilize these metastable films.[29] Moreover, in the absence of a hard bounding surface, the film liquid can evaporate (or the vapor can condense), making it difficult to maintain a free liquid film during the course of a simulation.

In our previous works, we determined the disjoining-pressure isotherms for free one-component Lennard−Jones (LJ) thin films,[27] one-component water, and two-component water/inert gas films.[28] In all cases, Π was negative, corresponding to attractive forces, as expected. On the other hand, experimental thin films are stabilized by surface-active molecules, and positive values of Π are obtained. Thus, we perform here MC simulations (described below in greater detail) of surfactant-stabilized thin films. In our previous work with water and inert-gas two-component films, we discussed the necessity of an inert gas to maintain a constant chemical potential of the solvent (water) as the film is thinned.[28] We showed that in contrast to one-component pure-solvent films, a two-component system permits a constant-chemical-potential reservoir for the solvent to be in equilibrium with the thin film, thus mimicking the experimental measurements.[6−16] Here, in an analogous manner, we choose our simulated surfactant-stabilized film systems to be surrounded by inert-gas molecules.

Simulation Details

Potential Models. Several models for surfactants, based on LJ interactions, are available in the literature.[30−32] A basic feature in these intermolecular potential models is that the corresponding LJ parameters are adjusted such that head molecules of the surfactant prefer the solvent and the tail molecules prefer to be away from the solvent. Thus, the surfactant molecule as a whole prefers to reside at the solvent/vapor interface. Each of the four types of atoms (solvent (s), inert gas (g), surfactant head (h), and surfactant tail (t)) interacts with another atom by a cut and shifted LJ potential. All $\sigma_{i,j}$ are equal ($\sigma_{s,s} = \sigma_{s,h} = \cdots \equiv \sigma$). $\epsilon_{i,j}/k$ (k is the Boltzmann constant) values for each $\{i, j\}$ pair are given in column 3 of Table 1. Subsequent parameters and variables are nondimensionalized with respect to σ and $\epsilon_{s,s}$. ϵ values are chosen such that the surfactant head is attracted more to the solvent than to the inert gas (or itself), and the interaction of the surfactant tail with the inert gas is more favorable than that with the solvent. $\epsilon_{g,g}$ is significantly lower than $\epsilon_{s,s}$ so that the critical point of the inert

* To whom correspondence should be addressed. Phone: 510-642-5204. FAX: 510-642-4778. E-mail: radke@cchem.berkeley.edu.

10.1021/jp0485791 CCC: $27.50
Published on Web 08/06/2004

TABLE 1: Model Parameters for Interatmoic Potentials

i	j	$\epsilon_{i,j}$ (K)	$r_{c;i,j}$ (σ)
s	s	300	2.5
s	h	400	2.5
s	t	150	2.5
s	g	300	$2^{1/6}$
h	h	300	2.5
h	t	300	2.5
h	g	300	$2^{1/6}$
t	t	300	$2^{1/6}$
t	g	400	2.5
g	g	50	2.5

gas is lower than that of the solvent. $\epsilon_{s,h}$ is larger than $\epsilon_{s,s} = \epsilon_{h,h}$. Thus, the surfactant head prefers to be solvated by the good solvent. Further adjustments to the interparticle potentials are made by adjusting the cutoff distance, $r_{c;i,j}$, for the LJ interaction between each pair of particles. The $r_{c;i,j}$ values for each type of pair are given in column 4 of Table 1 (in units of σ). From Table 1, it is clear that the solvent/inert-gas interactions are purely repulsive to make the inert gas insoluble in the solvent. Also, the purely repulsive interaction between tail segments of the surfactants prevents the aggregation or micellization of the surfactants in solution, while still allowing adsorption of the surfactant to the liquid/vapor interface. The reasons for such choices for $r_{c;s,g}$ and $r_{c;t,t}$ become clear later. In addition, surfactant headgroups are repelled from the inert gas so that the surfactants exhibit a negligible vapor pressure.

Each surfactant has 4 head and 4 tail atoms in sequence (H_4T_4), with each atom of the surfactant connected to the adjacent one by a finitely extensible harmonic spring whose potential is given by

$$u_{\text{spring}} = \begin{cases} {}^1/_2 k_s (r - r_0)^2; & 0.75\sigma \le r \le r_{c;s,s} \\ \infty; & \text{otherwise} \end{cases} \qquad (1)$$

where $k_s = 80.0$ (dimensionless), r is the distance between the adjacent atoms connected by the spring, and $r_0 = \sigma$.

Monte Carlo Simulation Method. In Figure 1, a thin liquid film is shown connected to a liquid reservoir via a curved meniscus. The liquid reservoir maintains constant chemical potentials of the surfactant and the solvent molecules similar to experiment, allowing the film thickness to vary by controlling the gas pressure, p_G, above the film. The disjoining pressure, Π, is defined as the difference between the pressure in the gas phase above the film, p_G, and the pressure in the homogeneous liquid reservoir, p_L. Following Winter,[34] we choose one simulation box to represent the flat part of the film (Box 1) and a second box to correspond to the liquid reservoir (Box 2), as illustrated in Figure 1. For our simulations, Box 2 is cubic with all the edge lengths being 13σ. Box 1 is elongated in the z-direction perpendicular to the interface ($40\ \sigma$) and $14\ \sigma$ in the other two directions. Periodic boundary conditions, with the nearest-neigbhor image convention, are applied in all directions in both boxes.

In Box 1, we randomly place a fixed number of solvent and surfactant molecules in the center of the box corresponding to a liquidlike density at the center of the film. The gas space above this liquid region is initially filled with inert-gas molecules. Box 2 is initially comprised of solvent and surfactant molecules at a liquid density. First, we equilibrate each simulation box separately for a total of 60 million steps, where each step is one particular type of move for a particle. For solvent and inert-gas molecules, the usual Metropolis random-walk algorithm is used.[35] The surfactant molecules are moved according to the continuum configurational bias algorithm.[36,37] To speed up the equilibration of the surfactant, we further use identity-swap moves,[38] whereby each segment of the surfactant swaps identity with eight (corresponding to H_4T_4) solvent molecules in the same simulation box.

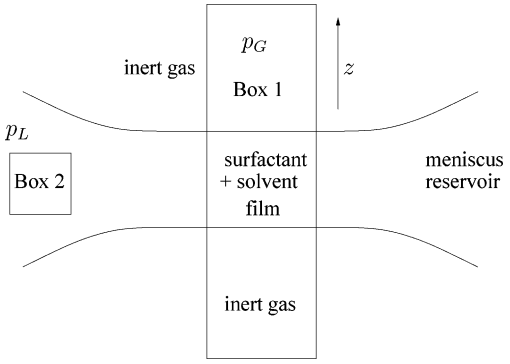

Figure 1. A schematic of the simulation system for a thin film in contact with a liquid reservoir. The simulation Box 1 is placed in the flat part of the thin film and simulation Box 2 in the liquid reservoir.

The next step is to equilibrate the chemical potential of all three species in the two boxes. Winter determined that, if species exchange is allowed in Box 1 as in Gibbs-ensemble Monte Carlo (GEMC) (to equilibrate the chemical potential), then the film evaporates/condenses, lowering its free energy, and bulk liquid−vapor coexistence without interfaces is simulated.[34] Solution of the film-evaporation problem was to perform purely a canonical-ensemble simulation in Box 1 and to let this box act as a chemical-potential reservoir for Box 2. Thus, species-exchange moves are tried between the two boxes. However, the moves are accepted only in Box 2. Both the solvent and the inert-gas molecules are exchanged between the two boxes (with the move accepted and, thus, the corresponding configuration is updated only in Box 2) with the acceptance probability given by particle-exchange moves in GEMC.[39,40] For surfactant molecules, a random exchange is highly improbable. Thus, we use identity-exchange moves between a random surfactant in one of the boxes and eight solvent molecules in the other box.[38] If the tail molecules have a favorable interaction with each other, the surfactants tend to cluster together, and the identity-swap moves (and hence, the equilibration between boxes) become very improbable. For this reason, the tail−tail interactions are chosen to be purely repulsive inhibiting the formation of surfactant clusters. In this second part of the simulation lasting about 50 million steps, we additionally attempt particle exchanges between boxes (accepted only in Box 2), along with the above-mentioned moves within a box.

Once Box 2 has equilibrated with Box 1, the pressure can be calculated in each box (isotropic pressure in Box 2 and normal pressure in Box 1), and Π of the film is determined. However, we use a ghost-volume fluctuation algorithm,[34] in combination with the moves mentioned above, to determine Π. This algorithm is similar in idea to the detailed-balance method for chemical-potential determination developed by Fay et al.[41] We discuss this method in greater detail shortly. The final production run is carried out for 100 million steps.

Results

Isotherm 1. First, we simulate a thick film, Film 1, consisting of 1646 solvent (s) molecules, 60 surfactant (a) molecules, and 320 inert-gas (g) particles. The final equilibrated nondimensional density profiles for the three components are shown in Figure 2. For the surfactant molecules, the center-of-mass (assuming all segments are of equal mass) density profile is plotted. From

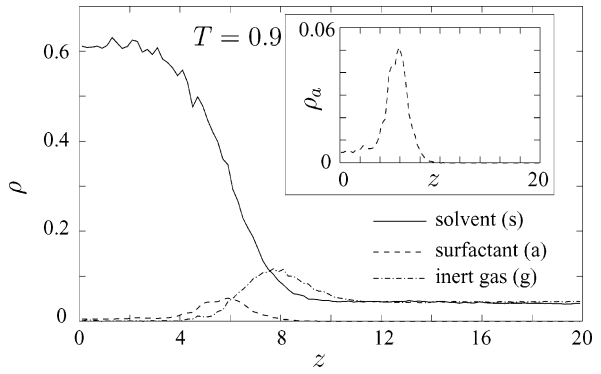

Figure 2. Density profile in Box 1 for film 1 ($h = 11.4$) for the three components. $z = 0$ represents the center of the film. The inset shows the surfactant density profile in greater detail.

the figure, it is clear that the surfactant molecules (dashed line) are positively adsorbed at the interface. Thus, the model surfactant does exhibit surface-active behavior. The inset shows the surfactant density profile in greater detail. Additionally, the inert-gas molecules (dashed−dotted line) have an increased density near the interface due to the presence of surfactants near the interface (the tail molecules of the surfactant have a favorable interaction with the inert gas). On the other hand, the inert gas has negligible solubility in the liquid region of the film and in the bulk liquid reservoir of Box 2.

Since the interaction between tail atoms of the surfactant is purely repulsive, the adsorption behavior of our model surfactants is different than that of the model surfactants chosen by Tomassone et al.[32] Their surfactants show a surface-phase transition similar to that of a Frumkin isotherm[33] in that the surfactant adsorption is negligible until a specific bulk concentration is reached where the adsorption increases precipitously (and plateaus off at higher surfactant concentrations). Such adsorption phase transitions are due to favorable interactions between the surfactant tail molecules. Since the tail atoms of the model surfactants in our work do not have attractive interactions, we expect a lower surfactant adsorption at a pure solvent liquid/vapor interface than that obtained by Tomassone et al.[32] However, in our case, the presence of tail-attractive inert-gas molecules enhances the adsorption of the surfactant molecules at the liquid/gas interface.

For Film 1 in Figure 2, the equilibrated solvent and surfactant densities in Box 2 are 0.631 ± 0.022 and $4.93 \times 10^{-3} \pm 1.03 \times 10^{-3}$, respectively. Within the accuracy of the simulation, both of these densities are identical, respectively, to the solvent and the surfactant densities in the liquid region of Film 1. For a thick film with a distinct homogeneous liquid region in the center, we expect the component densities in the homogeneous liquid reservoir to be the same as those in the liquid region of the film (due to equality of chemical potentials and the fact that such a thick film represents bulk phase equilibrium). Thus, the identical surfactant and solvent densities also serve as a check on the simulation consistency. Further, we expect the orientation of surfactant molecules to be random (unaffected by the presence of the interfaces) at the center of the film corresponding to bulk solution. The angular distribution of the angle, θ, that the end-to-end vector of a surfactant molecule makes with the outward normal to the interface (e.g., when $\theta = 0°$, the end-to-end vector is perpendicular to the interface with the tail atoms on the vapor side of the interface) is shown in Figure 3 by closed circles for surfactant molecules near the interface ($|z| = 6 \pm 0.5$), by open circles at the center of Box 1 ($z = 0 \pm 0.5$), and by open squares in Box 2. Of course,

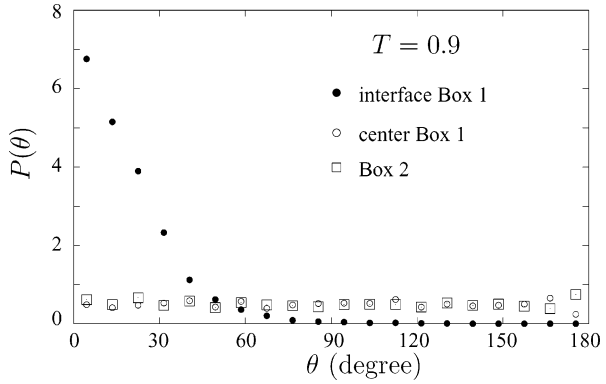

Figure 3. Comparison of the end-to-end orientational distribution of surfactant molecules in Film 1 at the interface (closed circles), in the center of the film (open circles), and in the liquid reservoir in Box 2 (open squares). The normalization integral is $\int_0^\pi P(\theta) \sin\theta \, d\theta = 1$.

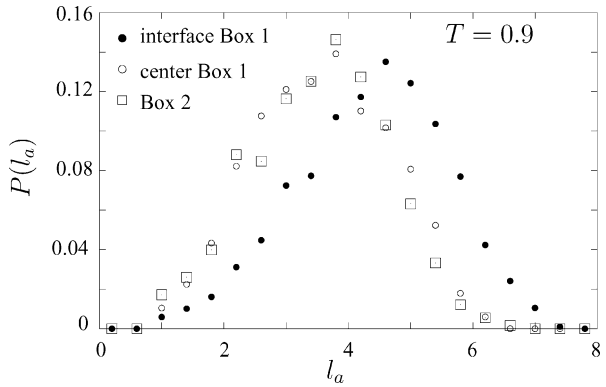

Figure 4. Comparison of the end-to-end length distribution of surfactant molecules in Film 1 at the interface (closed circles), in the center of the film (open circles), and in the liquid reservoir in Box 2 (open squares).

since Box 2 lacks an interface, the orientation is arbitrary with respect to the z axis of Figure 1. Clearly, the orientation of the surfactant molecules is random at the center of Film 1 and also in Box 2 that is in equilibrium with the film. In contrast, the adsorbed surfactant molecules are preferentially oriented perpendicular to the interface with the tail atoms in the gas phase, as expected.

The corresponding distributions of the end-to-end length of the surfactant molecules (l_a) is shown in Figure 4, where the symbols are the same as in Figure 3. In the homogeneous Box 2, the most probable value for l_a is approximately 4, which is larger than $\sqrt{7} = 2.65$, the value for a long, self-avoiding freely jointed chain.[42] Clearly, the surfactant molecules are somewhat elongated near the interface, whereas the length distribution at the center of Film 1 is almost identical with that in the homogeneous Box 2. Elongation is due to surface-induced orientation and the presence of nearby adsorbed surfactant heads. For Film 1, the surface excess adsorption of surfactant molecules (Γ_a) is 0.12 ± 0.01 at the solvent Gibbs dividing surface (where the solvent adsorption is zero). This value corresponds to roughly one surfactant molecule per 3×3 interfacial area.

In GEMC, the acceptance probability for two simulation boxes with a pressure difference of ΔP is given as[40]

$$\mathscr{P}_{\text{vol}} = \min\left\{1, \exp\left(-\beta(\Delta U_1 + \Delta U_2 + \Delta P \Delta V) + N_1 \ln\frac{V_1 + \Delta V}{V_1} + N_2 \ln\frac{V_2 - \Delta V}{V_2}\right)\right\} \quad (2)$$

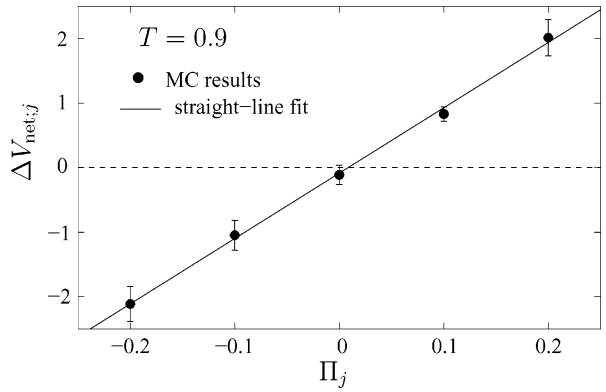

Figure 5. Net volume transferred (if such a transfer were allowed) from Box 1 to Box 2 for Film 1 as a function of five different trial values of Π.

where ΔU_i is the change in potential energy of Box i due to the change in volume, V_i is the volume of Box i, N_i is the total number of particles in Box i, ΔV is the attempted change in volume with sign defined such that ΔV is positive if the attempted change increases the volume of Box 1, and $\Delta P = p_1 - p_2$. If the attempted volume fluctuation for Box 1 is only along the direction perpendicular to the interface keeping the area of Box 1 constant and is isotropic for Box 2, p_1 can be identified with p_N and p_2 becomes p_L. Accordingly, $\Delta P \equiv \Pi$.

To calculate Π for a film using the above procedure, we choose five different values of Π, say Π_j where $j = 1$ to 5. For each Π_j value, we attempt volume-fluctuation moves and check the acceptance using eq 2. However, instead of accepting such volume moves and thereby updating configurations, we merely keep track of the net fluctuation in volume, $\Delta V_{\text{net};j}$, for each j that would have occurred if these moves were actually allowed. Subsequently, we plot $\Delta V_{\text{net};j}$ for each Π_j as shown in Figure 5 for Film 1. A best-fit straight line to the simulated values of $\Delta V_{\text{net};j}$ versus Π_j is shown as a solid line in the figure. The intersection of this line with the $\Delta V_{\text{net};j} = 0$ axis (dashed line in Figure 5) gives the required value of Π for this film as 0.008 ± 0.020.

Thus, Film 1 represents a thick film with Π close to zero (an infinitely thick film, of course, has $\Pi \equiv 0$). This finding is in agreement with the results above that the component densities in the center of Film 1 are very close to the corresponding densities in the homogeneous Box 2 and that the film is thick enough for the orientation of surfactant molecules in the center of the film to be random.

Film 1, and more importantly the homogeneous liquid in Box 2 in equilibrium with Film 1, establishes the conditions that determine a particular disjoining-pressure isotherm. In particular, since the homogeneous liquid in Box 2 represents an infinite reservoir of surfactant and solvent, the solvent and the surfactant chemical potential obtained for Film 1 must be maintained as constant as the films are thinned to mimic actual experimental situations. As in thin-film balance measurements,[6−16] this is achieved by changing the pressure exerted by inert-gas molecules in Box 1. Now, since the solubility of the inert gas in the solvent is negligible (as evidenced in Figure 2), a constant surfactant and solvent density in Box 2 (for all thin films) implies that the chemical potentials (and also the pressure in Box 2) of these two components are essentially constant. Thus, we obtain a film of different thickness on the same isotherm by performing an iterative procedure whereby different numbers of surfactant and inert-gas molecules are placed in Box 1 (the canonical ensemble) for a given number of solvent molecules until the equilibrated densities of the solvent and the surfactant molecules in Box 2 equal the desired values (i.e., those obtained for Film 1).

Ideally, of course, this iterative procedure could be eliminated by performing a canonical-ensemble simulation in Box 2 and allowing Box 1 to equilibrate with it. However, as mentioned above, allowing actual particle transfer from or to Box 1 eventually destroys the film.

Table 2 shows in columns 2 to 4, respectively, the number of solvent ($N_{s;1}$), surfactant ($N_{a;1}$), and inert-gas molecules ($N_{g;1}$) in Box 1 for 10 different films (including Film 1). Films 1 to 5 are on the same isotherm (isotherm 1), whereas Films 6 to 10 are on a different isotherm with a higher surfactant concentration to be discussed below. Columns 5 to 7 report the equilibrated solvent ($\rho_{s;2}$), surfactant ($\rho_{a;2}$), and inert-gas densities ($\rho_{g;2}$) in Box 2 for each of the films. The numbers in parentheses represent the error in the last significant digits. Within the errors, both the solvent and the surfactant densities are the same for the different films. Further, the solubility of inert gas in the liquid phase is negligible. Columns 8 and 9 report the vapor densities in Box 2 for both the solvent ($\rho_{s,v;1}$) and the inert-gas molecules ($\rho_{g,v;1}$), respectively. The surfactant molecules are nonvolatile. The value of Π for each of the films is shown in column 10.

Following de Feijter,[43] the film thickness, h, is defined by a Gibbsian-motivated step-density profile between the equilibrium solvent liquid density ($\rho_{s;2}$) and the equilibrium solvent vapor density ($\rho_{s,v;1}$) and zero adsorption at the dividing surface. Column 11 of Table 2 gives the film thickness so calculated in units of σ.

The disjoining pressure for isotherm 1, $\Pi(h)$, is plotted in Figure 6, as Films 1 to 5 (closed circles). Clearly, the disjoining pressure is positive and increases monotonically as the film thickness decreases. In contrast, free thin films without any stabilization (whether due to surface-active agents or electrostatic) exhibit negative values of Π in simulations.[27,28] For the present models of the solvent and the inert-gas molecules, we performed the MC simulations without the surfactants present

TABLE 2: Relevant Properties for Films Simulated[a]

	$N_{s;1}$	$N_{a;1}$	$N_{g;1}$	$\rho_{s;2}$	$\rho_{a;2}/10^3$	$\rho_{g;2}/10^3$	$\rho_{s,\,v;1}$	$\rho_{g,\,v;1}$	Π	h
Film 1	1646	60	320	0.631(22)	4.93(1.03)	0.57(49)	0.041(4)	0.042(3)	0.008(20)	11.4
Film 2	1371	60	350	0.640(18)	5.01(1.36)	0.44(32)	0.042(3)	0.041(3)	0.010(18)	8.9
Film 3	1097	60	400	0.634(22)	4.48(1.26)	0.56(47)	0.034(3)	0.045(2)	0.040(25)	7.1
Film 4	987	55	420	0.624(24)	4.43(1.18)	1.13(74)	0.030(4)	0.048(2)	0.055(21)	6.5
Film 5	768	40	450	0.627(18)	4.30(1.18)	0.86(55)	0.031(2)	0.054(3)	0.060(18)	4.5
Film 6	1646	82	320	0.599(22)	7.96(1.27)	1.21(58)	0.034(5)	0.039(3)	0.011(17)	12.5
Film 7	1371	77	360	0.603(19)	8.74(1.23)	1.07(68)	0.038(3)	0.038(3)	0.032(15)	9.6
Film 8	1097	73	420	0.600(23)	8.91(1.34)	1.77(93)	0.035(3)	0.042(4)	0.047(17)	7.4
Film 9	987	68	425	0.610(19)	7.89(1.45)	0.87(77)	0.038(4)	0.042(3)	0.042(18)	6.1
Film 10	878	58	460	0.601(20)	7.97(1.21)	2.07(97)	0.031(4)	0.053(3)	0.061(19)	5.7

[a] Films 1 to 5 correspond to isotherm 1, and films 6 to 10 correspond to isotherm 2.

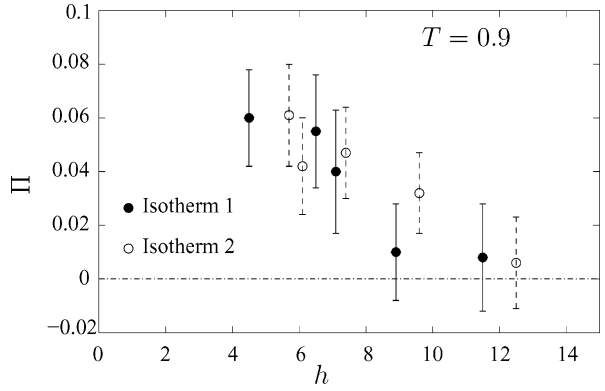

Figure 6. Disjoining-pressure isotherms for films with two different surfactant concentrations in the homogeneous reservoir (isotherm 1 and isotherm 2).

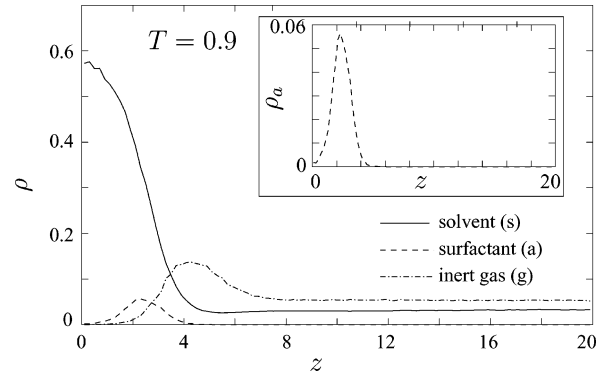

Figure 7. Density profile in Box 1 for Film 5 for the three components. $z = 0$ represents the center of the film. The inset shows the surfactant density profile in greater detail.

(using a similar number of molecules as in Films 1 to 5). Thicker films (out to $h \approx 8$) displayed $\Pi = 0$, and thinner ones were unstable. Without the stabilizing surfactant molecules, we were not able to obtain a range of film thicknesses with different values of Π.

Figure 7 graphs the solvent, center-of-mass surfactant, and the gas density profiles for the thinnest Film 5 with $h = 4.5$. The solvent density profile no longer reaches a constant plateau at the film center. The surfactant and the gas adsorption densities remain centered at the solvent-defined Gibbs dividing surface. Importantly, the widths of both the gas and surfactant profiles do not change significantly from those in Figure 2 for a thick film with no disjoining forces present. Detailed comparison of the surfactant density profiles in the insets of Figure 2 and 7, however, shows that the surfactant density at the center of Film 5 is smaller than that in thick Film 1 by a factor of about 2. This means that as the films are thinned, some bulk surfactant is expelled.

For a random orientation of surfactant molecules away from the interface, the head (h) and the tail (t) number densities of the surfactant molecules must be identical. Thus, we plot $\rho_h - \rho_t$ as a function of z in Figure 8 for Films 1 to 5. Film 1 does indeed have equal h and t segments at the center confirming the presence of bulk surfactant. Thinner films have a larger number of surfactant headgroups than tail groups in the liquidlike center of the corresponding films, and this difference increases significantly as the films thin. This is simply due to the surfactant headgroups in the liquid part of the interface overlapping with those adsorbed on the opposing interface. Overlap commences already in Film 2 of Figure 8 at $h \approx 8$. Our simulations reveal little change in either the adsorbed

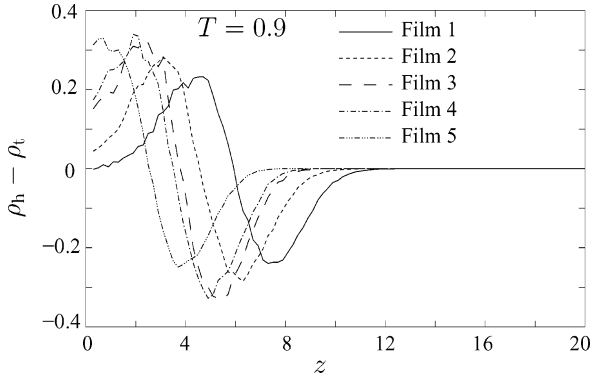

Figure 8. Difference in the segment densities as a function of z of the head and the tail segments of surfactant molecules for Films 1 to 5.

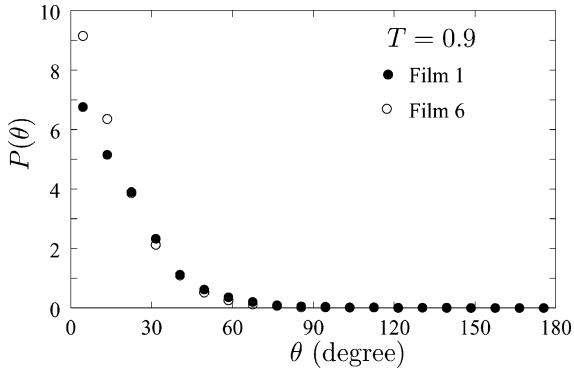

Figure 9. A comparison of the end-to-end orientational distribution of the surfactant molecules in thick films of different concentration.

surfactant orientation distribution, $P(\theta)$ in Figure 3, or the end-to-end length distribution, $P(l_a)$ in Figure 4, as the film thins. This means that the overlapping headgroups in Films 2 to 5 are not compressed or reoriented compared to their configurations at a single interface. Overlap is primarily due to interpenetration of the headgroups emanating from the opposing interfaces. Surfactant tail groups remain unaltered as the films are thinned. Results for Film 5 in Figures 7 and 8 indicate that the center of this film consists primarily of perpendicularly oriented, elongated, and interdigitated adsorbed surfactant headgroups with few bulk surfactant molecules. In combination, Figures 3, 4, 7, and 8 suggest that as the films thin the solvated headgroups interact entropically resulting in an increase in Π.

Isotherm 2. Now we consider the effect of increasing the concentration of surfactant molecules, thus, increasing Γ_a of the surfactant molecules. Film 6 in Table 2 shows a film with increased surfactant concentration. From the result that Π for Film 6 is close to zero (column 10 of Table 2), we consider it to be a thick film for Isotherm 2 and, therefore, comparable to Film 1 (thick film for Isotherm 1). Γ_a for Film 6 is 0.16 ± 0.01. This corresponds to one surfactant molecule per 2.5×2.5 interfacial area. From Films 1 and 6, we observe that Γ_a increases by about 30% for an 80% increase in $\rho_{a;2}$, indicating that the surfactants are below the monolayer coverage but outside the Henry's region. Figure 9 compares the orientational distribution of surfactant molecules at interfaces for Films 1 (closed circles) and 6 (open circles). Note that when the open circles are not visible for certain angles, they are hidden behind the closed circles. For smaller angles ($\theta = 0$ is normal to the interface, with the tail molecules in the gas phase) it is clear that at higher Γ_a (Film 6), the orientational distribution is slightly more sharply peaked.

Correspondingly, Figure 10 plots the surfactant-length distribution of Films 1 and 6 near the interface. In accordance with

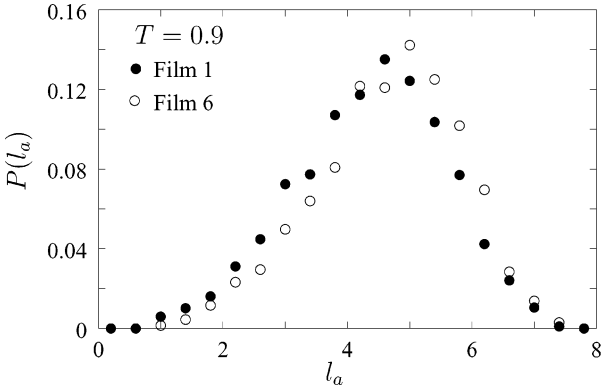

Figure 10. A comparison of the end-to-end length distribution of the surfactant molecules in thick films of different concentration.

the orientational distribution of Figure 9, the peak for $P(l_a)$ shifts to the right for Film 6. Thus, Figures 9 and 10 show that the surfactants are slightly more "stretched" for the film with a higher surface coverage of surfactant. Similar results were also obtained by Tomassone et al. for a large number of surfactant coverages.[32] We return to this point shortly.

Similar to isotherm 1, we simulate disjoining pressures for thinner films along isotherm 2 at the higher surfactant concentration corresponding to Film 6. Films 7 to 10 on isotherm 2 are documented in Table 2. Π as a function of h for isotherm 2 is graphed as open circles in Figure 6. Again, Π is positive and increases monotonically as the films thin. The tendency for a slightly larger stretch of surfactants, as mentioned above, is maintained for thin films of isotherm 2 as compared to thin films of isotherm 1. This stretching allows the surfactants on the opposite interfaces of thin films at higher surfactant concentration to obstruct each other at larger film thickness than for the surfactant solution at lower coverage. Additionally, at higher coverages, the surfactants are closer together; this is expected to increase the entropic penalty for confinement.

Discussion

Interaction forces in surfactant-stabilized free thin films can be classified into attractive and repulsive. Attractive interaction forces consist of those due to Hamaker (i.e., van der Waals)[27,28] and those due to depletion aggregation.[44−46] Repulsive forces with nonionic surfactants include the following: peristaltic, protrusion, and headgroup overlap (i.e., steric stabilization).[26,47] Hydrophobic and hydrophilic interaction forces[46] are not pertinent to our LJ films.

Attractive van der Waals or Hamaker forces in surfactant-free LJ films appear to be larger in magnitude than those predicted by classical theory for the film thickness studied in this work.[27] We cannot employ those results directly here because of gas and surfactant adsorption at the interface. Moreover, the thermodynamics of single-component films is not identical with that for multicomponent films.[28] Hence, we cannot identify separately the contribution due to Hamaker forces in our films by, for example, simulating surfactant-free films.

Depletion attraction in films confined between hard walls is argued to arise from an osmotic stress induced by size rejection of surfactant molecules from the film.[44−46] Although we observe some depletion of bulk surfactant from the simulated films, it is not major and does not contribute to the calculated disjoining pressures. As importantly, the mechanism(s) by which solute molecules are rejected from soft free thin films and the resulting magnitude of the depletion attraction may not be directly analogous to those for confined films.

Repulsive peristaltic and protusion forces refer respectively to the configurational confinement of film-thickness fluctuations (i.e., fluctuations in the location of the Gibbs dividing surface) and surfactant-molecule fluctuations normal to the interface as the film thins.[26,47] The diffuse spreading in the solvent−density profiles in Figures 2 ($h \geq 11.5$) and 7 ($h = 4.5$) is quite similar. Likewise, the breadths of the surfactant density profiles in Figures 2 and 7 are not materially altered over the range of film thicknesses studied. Unfortunately, the diffuseness of an ensemble-average density profile does not gauge the fluctuations in that profile. Our simulations do not permit an assessment of the importance of peristaltic and protrusion forces.

Steric stabilization is the classic mechanism by which adsorbed polymer imparts stability to colloidal suspensions.[47] As the extremities of the adsorbed molecules on the two interfaces encounter each other, entropic confinement leads to a repulsive interaction force. From the headgroup overlap seen in Figure 8 and the resulting repulsive disjoining forces (cf. Figure 6), entropic steric stabilization clearly is operative. Indeed, in the thinnest films studied ($h \approx 5$), the film center consists primarily of overlapping headgroups. Also, as the adsorption coverage is increased at the higher surfactant concentration, the calculated disjoining pressures increase consistent with increased steric repulsion. In our simulations, however, the statistical uncertainties in Π preclude a clear distinction between the two different concentration isotherms in Figure 6.

Although the adsorbed surfactant molecules in our model system are oriented and elongated into a brush-like headgroup structure, Alexander/de Gennes theory[48,49] for entropically confined, end-grafted polymer brushes does not apply. The LJ surfactant molecules in this work are entropically constrained between the two interfaces of the thin films. However, they are neither end grafted to the interface nor irreversibly adsorbed. They are free to move and desorb to maintain equilibrium with the bulk reservoir. Also, as discussed earlier, the overlapping headgroups are not compressed during film thinning. Rather, overlap is due to interdigitation. In the theory of Alexander and de Gennes, entropic confinement leads to compression of the opposing polymer brush. For these many reasons, Alexander/de Gennes theory is not pertinent to our system.

In principle, the disjoining-pressure isotherms in Figure 6 include all the force contributions enumerated above. However, we have no reliable theories to separate these contributions. Nor can the various interaction forces be separated in the simulations. Indeed, it is not clear that individual contributions to thin-film forces can even be separated conceptually, as they are not likely to be additive.

Conclusions

In this work, we extend our previous calculations of disjoining-pressure isotherms for two-component water/inert gas thin films to include a film-stabilizing surface-active agent. We reiterate the importance of the inclusion of inert-gas molecules to allow an infinite solvent/surfactant mixture reservoir mimicking actual thin-film balance experiments. To reduce the computational complexity, yet still allow for a qualitatively correct picture of surfactant behavior, we chose LJ potential models for all the molecules present in the system. The model surfactant does indeed exhibit a surface-active behavior at the solvent/inert-gas interface and remains nonvolatile and nonaggregating in the bulk liquid. We observe that the surfactant molecules

are elongated and perpendicular to the interface at the interface and randomly oriented in bulk. Simulation of thinner films for a particular isotherm requires an iterative procedure to obtain the same solvent and surfactant chemical potentials (or densities, since the density of the inerts is negligible in the liquid phase) for films of different thicknesses. As the films are thinned, the orientation and structure of surfactant molecules at the interface are not affected significantly, nor are the breadths of the solvent and surfactant density profiles.

For the surfactant-stabilized films studied here, the disjoining pressure is positive and increases monotonically as the films are thinned over the range of thicknesses studied. This is, in part, due to a repulsive entropic overlap and entropic confinement of solvated surfactant headgroups that interdigitate with surfactant headgroups in the surfactant layer adsorbed on the opposite interface. We simulate two isotherms at two different surfactant concentrations and interfacial adsorptions of the surfactant molecules. The surfactant molecules are more elongated at the interface and have a higher surface coverage at the higher surfactant concentration. This leads to a slightly larger repulsive Π value than the isotherm with a lower surfactant concentration in the bulk. However, the distinction is blurred by the statistical errors of our simulation.

References and Notes

(1) Davis, H. T.; Scriven, L. E. *Adv. Chem. Phys.* **1982**, *49*, 357.
(2) Derjaguin, B. V.; Churaev, N. V. *Colloid J. USSR* **1976**, *38*, 402.
(3) Derjaguin, B. V.; Churaev, N. V. *J. Colloid Interface Sci.* **1978**, *66*, 389.
(4) Kruglyakov, P. M. *Thin Liquid Films*; Ivanov, I. B., Ed.; Marcel Dekker, Inc.: New York, 1988; Chapter 11, p 767.
(5) Ivanov, I. B. *Colloids Surf. A* **1997**, *128*, 155.
(6) Mysels, K. J.; Jones, M. N. *Discuss. Faraday Soc.* **1966**, *42*, 42.
(7) Exerowa, D.; Kolarov, T.; Khristov, K. H. R. *Colloids Surf.* **1989**, *22*, 171.
(8) Kolarov, T.; Cohen, R.; Exerowa, D. *Colloids Surf.* **1989**, *42*, 49.
(9) Bergeron, V; Radke, C. J. *Langmuir* **1992**, *8*, 3020.
(10) Bergeron, V; Radke, C. J. *Colloid Polym. Sci.* **1995**, *273*, 165.
(11) Karraker, K. A.; Radke, C. J. *Adv. Colloid Interface Sci.* **2002**, *96*, 231.
(12) Exerova D.; Zacharieva, M. *Research in Surface Forces*; Derjaguin, B. V., Ed.; Consultants Bureau: New York, 1972; Vol. 4, p 253.
(13) Bergeron, V.; Waltermo, A.; Claesson, P. M. *Langmuir* **1996**, *12*, 1336.
(14) Sedev, R.; Nemeth, Z.; Ivanova, R; Exerowa, D. *Colloids Surf. A* **1999**, *149*, 141.
(15) Cascao Pereira, L. G.; Johansson, C.; Blanch, H. W.; Radke, C. J. *Colloids Surf. A* **2001**, *186*, 103.
(16) Bergeron, V.; Langevin, D.; Asnacios, A. *Langmuir* **1996**, *12*, 1550.
(17) Gallego, L. J.; Rey, C.; Grimson, M. J. *Mol. Phys.* **1991**, *74*, 383.
(18) Magda, J. J.; Tirrel, M.; Davis, H. T. *J. Chem. Phys.* **1985**, *83*, 1888.
(19) Dickman, R.; Anderson, P. E. *J. Chem. Phys.* **1993**, *99*, 3112.
(20) Jimenez, J.; Rajagopalan, R. *Eur. Phys. J. B* **1998**, *5*, 237.
(21) Berard, D. R.; Attard, P.; Patey, G. N. *J. Chem. Phys.* **1993**, *98*, 7236.
(22) Luzar, A.; Bratko, D.; Blum, L. *J. Chem. Phys.* **1987**, *86*, 2955.
(23) Shinto, H.; Miyahara, M.; Higashitani, K. *J. Colloid Interface Sci.* **1999**, *209*, 79.
(24) Forsman, J.; Jonsson, B.; Woodward, C. E. *J. Phys. Chem.* **1996**, *100*, 15005.
(25) Wang, J.-C.; Fichthorn, K. A. *Colloids Surf.* **2002**, *206*, 267.
(26) Israelachvili, J. N.; Wennerstrom, H. *J. Phys. Chem.* **1992**, *96*, 520.
(27) Bhatt, D.; Newman, J.; Radke, C. J. *J. Phys. Chem. B* **2002**, *106*, 6529.
(28) Bhatt, D.; Newman, J.; Radke, C. J. *J. Phys. Chem. B* **2003**, *107*, 13076.
(29) Chambers, K. T.; Radke, C. J. *Interfacial Phenomena in Petroleum Recovery*; Morrow, N. R., Ed.; Marcel Dekker Inc.: New York, 1990; p 211.
(30) Telo da Gama, M. M.; Gubbins, K. E. *Mol. Phys.* **1986**, *59*, 227.
(31) Smit, B.; Schlijper, A. G.; Rupert, L. A. M.; van Os, N. M. *J. Phys. Chem.* **1990**, *94*, 6933.
(32) Tomassone, M. S.; Couzis, A.; Maldarelli, C. M.; Banavar, J. R.; Koplik, J. *J. Chem. Phys.* **2001**, *115*, 8634.
(33) Adamson, A. W.; Gast, A. P. *Physical Chemistry of Surfaces*: John Wiley and Sons: New York, 1997; Chapter 5.
(34) Winter, S. J. Ph.D. Dissertation, University of California, Berkeley, 1999; Chapters 3 and 4.
(35) Metropolis, N.; Rosenbluth, A. W.; Rosenbluth, M. N.; Teller, A. H.; Teller, E. *J. Chem. Phys.* **1953**, *21*, 1087.
(36) Siepmann, J. I.; Frenkel, D. *Mol. Phys.* **1992**, *75*, 59.
(37) Frenkel, D.; Mooij, G. C. A. M.; Smit, B. *J. Phys.: Condens. Matter* **1992**, *4*, 3053.
(38) Wijmans, C. M.; Smit, B. *J. Chem. Phys.* **2001**, *114*, 7644.
(39) Panagiotopoulos, A. Z. *Mol. Phys.* **1987**, *61*, 813.
(40) Panagiotopoulos, A. Z.; Quirke, N.; Stapleton, M.; Tildesley, D. J. *Mol. Phys.* **1988**, *63*, 527.
(41) Fay, P. J.; Ray, J. R.; Wolf, R. J. *J. Chem. Phys.* **1994**, *100*, 2154.
(42) Rodriguez, F. *Principles of Polymer Systems*; McGraw Hill: New York, 1970; p 148.
(43) de Feijter, J. A. *Thin Liquid Films*; Ivanov, I. B., Ed.; Marcel Dekker: New York, 1988; Chapter 1.
(44) Asakura, S.; Oosawa, F. *J. Chem. Phys.* **1954**, *22*, 1255.
(45) Russel, W. B. *The Dynamics of Colloidal Systems*, The University of Wisconsin Press: Madison, WI, 1987; Chapter 2.
(46) Israelachvili, J. N. *Intermolecular and Surface Forces*, 2nd ed.; Academic Press: New York, 1995; Chapters 13 and 14.
(47) Napper, D. H. *Polymeric Stabilization of Colloidal Dispersions*; Academic Press: New York, 1983; Chapter 10.
(48) Alexander, S. J. *J. Phys. France* **1977**, *38*, 983.
(49) de Gennes, P. G. *Adv. Colloid Interface Sci.* **1987**, *27*, 189.